Applied Clay Science 252 (2024) 107341

Contents lists available at ScienceDirect

Applied Clay Science

journal homepage: www.elsevier.com/locate/clay

Research Paper

Influence of smectite clays' pores volume on isoniazid adsorption and release

Jessica de Carvalho Arjona [a,b], Carina Ulsen [c], Francisco Rolando Valenzuela-Diaz [a], Nicole Raymonde Demarquette [b,*]

[a] Departamento de Engenharia Metalúrgica e de Materiais, Escola Politécnica, Universidade de São Paulo, São Paulo 05508-030, Brazil
[b] Mechanical Engineering Department, École de Technologie Supérieure, Montréal, QC H3C 1K3, Canada
[c] Departamento de Engenharia de Minas e de Petróleo, Escola Politécnica, Universidade de São Paulo, São Paulo 05508-030, Brazil

ARTICLE INFO

Keywords:
Drug release
Clay pore volume
Isoniazid
Clay adsorption

ABSTRACT

Clays have been extensively utilized in various fields due to their remarkable adsorption properties. In pharmaceutical and medical applications, they serve as potential excipients in pills. Emerging research demonstrated their effectiveness as vehicles for controlling drug release. Little has been elucidated, however, regarding the optimal clay characteristics for such applications. Therefore, this study aimed to investigate the influence of clay pores volume on the adsorption of isoniazid (INH), a key drug in tuberculosis treatments worldwide. To achieve this, seven clays were investigated to examine the impact of pores volume on the adsorption and release of INH. Chemical characterization of the clays was conducted using X-ray fluorescence (XRF) and Infrared vibrational spectroscopy (IR), while their mineralogical composition was determined through X-ray diffraction (XRD) and their pore volume by BET method via N_2 adsorption/desorption isotherms. Additionally, the interaction between clay and INH was evaluated using FT-IR, XRD, and Thermogravimetric Analysis (TGA). Kinetic adsorption studies were performed to determine the time to reach the equilibrium saturation of the clay by the drug, which was found to be around three hours for all clays. By comparing the pore volume of the studied clays, it became apparent that the clay with an optimal pore volume of approximately 0.100 cm^3/g exhibited superior adsorption/retention compared to those with lower or higher volumes. Furthermore, in vitro INH release curves were obtained mimicking release conditions in the intestine (pH 7.4) for a duration of 5 h. It was clearly shown that the release of INH from the clays depend on the pore volume. Our results provided valuable insights into the optimal clay characteristics which would enhance the adsorption and release of INH.

1. Introduction

Over the last few years, clays have been used for adsorption of different organic molecules, like drugs (Kiaee et al., 2022; Peng et al., 2018; Zheng et al., 2019) in a wide range of applications varying from anticancer (Zheng et al., 2019) to antibacterial medicine (Peng et al., 2018; S. Wang et al., 2012). They have been studied as nanocarriers in pharmaceutical and medical fields due to their non-toxic, stable, and non-expensive nature (Carazo et al., 2018a; Carazo et al., 2018b; Carazo et al., 2017; Damasceno Junior et al., 2019; Peng et al., 2018; Zheng et al., 2019). Notably, smectites are among the clay samples mostly used for this kind of application (Sciascia et al., 2021).

Smectites ability to be used as nanocarriers, for controlled drug release, is governed by their physical structures (Sciascia et al., 2021). They belong to the group of phyllosilicates which present a 2:1 layered structure composed of two silicate tetrahedral sheets separated by an aluminum octahedral one; they are attached by sharing oxygen atoms as shown in Fig. 1a. Each layer is around 1 nm thick and up to two microns in width. The layers are attached by van der Waals forces and the spacing between them is filled with inorganic cations to counterbalance their negative surface charges. The gap between them is known as the interlamellar distance (Brigatti et al., 2006). The layers are stacked to form entities generally referred to as particles or tactoids, and the assembling of tactoids results in the formation of aggregates. Due to the various possible orientations and combinations of these particles, as well as, the varying sizes of voids between them, numerous different aggregates are formed (Nicola et al., 2021). That elucidates why clay samples are classified as porous materials, exhibiting different types of pores,

* Corresponding author.
E-mail address: NicoleR.Demarquette@etsmtl.ca (N.R. Demarquette).

https://doi.org/10.1016/j.clay.2024.107341
Received 22 September 2023; Received in revised form 7 March 2024; Accepted 12 March 2024
Available online 18 March 2024

including micropores, mesopores, and macropores. Micropores, with width up to 2 nm, form the interlayer space within the particles. Mesopores, ranging from 2 nm to 50 nm in width, along with macropores, with width higher than 50 nm, form the interparticle space within the aggregate (Shah et al., 2018). This study endeavors to investigate the porosity, in terms of total volume of the pores in the clay samples without going into the detailed contribution of each kind of pores.

The clay's swelling behavior in different solvents and their permeability to different molecules are affected by their chemical structure, porosity, and cation exchange capacity (CEC). CEC is defined as the capacity of a clay to replace its interlayer cations by the interlayer's ones available in the surrounding solution (Wang et al., 2020). Unfortunately, what governs the adsorption and release of drugs is not fully understood. Many theoretical studies of adsorption and desorption of drugs from clays have been done at the atomistic level (Borrego-Sánchez et al., 2021). On the other hand, most experimental studies found in the literature show different results regarding drug adsorption and release using different clays (Carazo et al., 2018a; Carazo et al., 2018b; Carazo et al., 2017, 2019; Damasceno Junior et al., 2019). With the results found in the present paper, the authors strongly believe that the volume of pores could have an influence on the adsorption and release of the drug.

During the adsorption process, the incorporation of the substance occurs on the clay surface or inside its pores (Zhu et al., 2016). This occurs in three steps: in the first step there is the diffusion of the drug molecules to the surface of the adsorbent; in the second step, these molecules flow into the pores; and, finally, in the third step, surface interaction between the adsorbent and the adsorbate takes place (Fig. 1d). In this last step, the interaction of clay/INH takes place in two possible ways. Either through cation exchange or via interaction forces such as van der Waals force or hydrogen bonding (Tan and Hameed, 2017). Fig. 1b and Fig. 1c show the two ways that the drug (represented in yellow) can interact with the clay. The drug can penetrate the interlamellar space (Fig. 1b), increasing the interlamellar distance and interact with the clay by cation exchange, or remain in the space between the tactoids and interact with it through hydrogen bonding or van der Waal forces (Fig. 1c) (Reinholdt et al., 2013). Thus, the nature of the investigated drug and its interaction with the clay is an important parameter in controlled drug release (Kiaee et al., 2022).

Drug delivery systems (DDS) must be developed to ensure that the active drug achieves its therapeutic effect (Tiwari et al., 2012). DDS can be separated into two main groups: those characterized by an immediate release (IR) and those that are characterized by modified release (MR). An example of MR is sustained release (SR), involving the gradual release of the drug over an extended period, to avoid the rapid release of a high amount of the drug at the beginning, referred to as burst release. Burst release may result in significant side effects worsening the treatment efficacy. SR can be achieved through various methods, such as, incorporating the drug into a vehicle that releases it at a controlled rate. In addition, this approach has the advantage of protecting the drug from environmental reactions, such as pH or enzymatic actions (Perrie et al., 2019).

Isoniazid (INH) is a highly water-soluble drug used as one of the first-line drugs for tuberculosis treatment; however, it presents poor bioavailability and causes strong side effects, which reduce the effectiveness of the treatment. To increase patient compliance with the treatment protocol, this drug would be a good candidate to be used in a controlled release system. A few studies have reported the use of clay and other inorganic particles as vehicles to control the release of INH (de Almeida et al., 2019), such as montmorillonite (Carazo et al., 2018b), halloysite (Carazo et al., 2017, 2019), palygorskite (Carazo et al., 2018a; Damasceno Junior et al., 2019), zeolite (Souza et al., 2021), and silica nanoparticles (de Almeida et al., 2019).

INH chemical structure is shown in Fig. 1e where the presence of pyridine ring and hydrazine groups can be seen. These two groups provide for cation exchange between the clay and the drug or an interaction via hydrogen bonding (Bhat et al., 2020; Kiaee et al., 2022; Zhu et al., 2016). Such interactions can potencially result in a certain percentage of INH being retained within the particles hindering its release (Souza et al., 2020). Most studies regarding INH-clay DDS report burst release behavior, which, in some cases, should be avoided. Furthermore, the use of hybrids clay/INH can prevent the INH degradation caused by the interaction with other anti-tuberculosis drugs commonly co-administered (Carazo et al., 2019).

Also, to the best of our knowledge, the influence of clay mineral characteristics, such as the pore volume, on the use of clays for drug release systems has not been studied. The only field in which this was explored is petrol or natural gas extraction (Feng et al., 2018), where gas

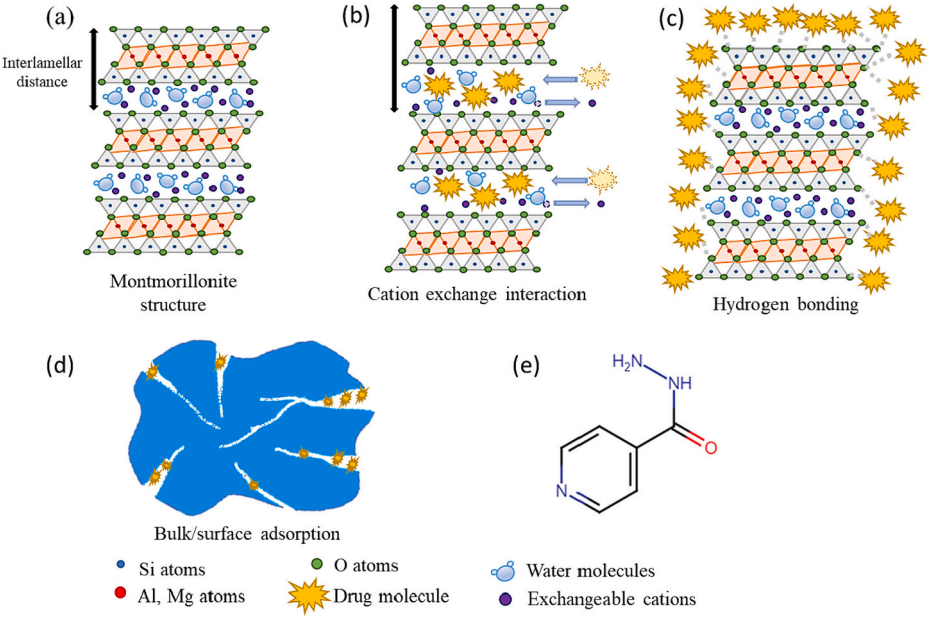

Fig. 1. Scheme of (a) clay structure, (b) clay/drug interaction by exchange interaction, (c) clay/drug interaction by hydrogen or van der Waals bonding, (d) bulk/surface adsorption of drugs by clay tactoids, and (d) isoniazid chemical structure.

adsorption in shale clay was examined (Wang et al., 2020). Therefore, this study investigates the influence of the pore volume of seven smectites to elucidate what are the factors that may govern the controlled release system efficiency in the case of INH. The results show that the volume of pores is an important clay characteristic that should be considered and mentioned in papers regarding this subject.

2. Materials and methodology

2.1. Materials and clay characterization

Table 1 presents the different clays that were used in this work. The INH used was an analytical standard purchased from Sigma-Aldrich.

The mineralogical composition of the clay particles was analyzed using XRD pattern obtained by the Empyrean Panalytical X-ray diffractometer system equipped with a kCu_{α} source. Scans were taken in the range of $2\Theta = 2.5° - 90°$ at 0.004°/min with an X-ray tube operated at 40–45 kV. The crystalline phases were identified by comparing the sample patterns with the International Centre for Diffraction Data (ICDD) and Inorganic Crystal Structure Database (ICSD).

Quantitative chemical analysis by X-Ray fluorescence (XRF) was conducted using a Zetium Malvern Panalytical instrument to determine the main compounds present in the clays including SiO_2, Al_2O_3, Fe_2O_3, MnO, MgO, CaO, Na_2O, K_2O, TiO_2, P_2O_5. For that lithium tetraborate infused samples were used. The loss on ignition (LOI) of the samples was assessed by gravimetry at 1020 °C for 2 h and represents the weight loss at a that temperature (Ulsen et al., 2019).

Inductively coupled plasma-optical emission spectroscopy (ICP OES iCap 6300 Duo by Thermo Scientific) was used to determine the amount of Pb and Cd in clays by multi-acid digestion preparation.

The surface area and pore volume of all clays were determined by low pressure N_2 adsorption/desorption isotherms at $T = 77$ K and relative pressure ranging from 0.05 to 1.0 (P/Po) (Shah et al., 2013), using the Micrometrics ASAP 2020 plus equipment. The clays' pore type was determined by the shape of N_2 adsorption/desorption curves (Sing et al., 1985), while the pore volume was determined by BJH (Barrett-Joyner-Halenda) model (Avnir and Jaroniec, 1989). Prior the test, the clays' samples were under the following process to ensure they were dried and free from any volatile contaminants. Each sample was 48-h drying at 90 °C to remove residual moisture, followed by resting in vacuum-sealed dissectors for 3 days. Then, the prepared samples were added into the Micrometris ASAP 2020 plus equipment to degas at 200 °C for 12 h.

2.2. Kinetics of adsorption

The adsorption of INH test was repeated three times as follows: 25 mL of a 4% (*w*/w) aqueous dispersion of each clay sample was subjected to 1550 rpm magnetic stirring for 15 min. A clay amount, sufficient to carry on the characterization tests after the sorption process, was chosen. Following this, an equal volume of an INH aqueous solution (0.02 mol/L) was added to the mixture. This concentration was chosen to ensure remaining below the presumed monolayer capacity of MMT, as shown by Carazo et al. (2018b). The system was subjected to magnetic stirring for six intervals 0.75 h, 1.5 h, 3 h, 6 h, 12 h, and 24 h, to evaluate the equilibrium saturation time of the clay by the drug. After each interval, the samples were centrifuged and the supernatant was analyzed using an ultraviolet-visible light spectrophotometer (UV–vis), while the decanted material was dried at 60 °C for further analyses, such as XRD, FTIR, and TGA.

To determine the amount of INH incorporated into the clays, an Agilent Cary 60 UV–Vis was used. For that, a calibration curve was obtained evaluating the measured absorbance of different INH solutions with known concentrations at a wavelength of 263 nm. A correlation of the INH concentration (C) with the measured absorbance (Abs) was obtained (Eq. 1).

$$Abs = 3.820 \bullet C, R^2 = 0.9999 \quad (1)$$

The amount of incorporated INH per gram of clay (Q_a) was obtained as the difference between the initial quantity of INH (Q_i) and the remained one (Q_m) in the supernatant after each interval (Eq. 2). Where Q_a represents the quantity of isoniazid adsorbed per gram of clay, Q_i is the initial quantity of INH in the solution at the beginning of the adsorption test, measured by UV–vis, Q_m is the quantity of INH that remained in the supernatant at the end of the test, measured by the UV–vis equipment, using the calibration curve, and m is the amount (in gram) of the clay used in the test.

$$Q_a = \frac{Q_i - Q_m}{m} \quad (2)$$

The experimental data were fitted to three different mathematical models to evaluate the adsorption kinetics of INH by MMT, namely pseudo-first order (PFO), pseudo-second order (PSO), and adsorption-diffusion model (ADM) given by Eq. 3, Eq. 4, and Eq. 5, respectively:

$$\frac{1}{q_t} = \left(\frac{k_1}{q_e}\right)\left(\frac{1}{t}\right) + \frac{1}{q_e} \quad (3)$$

$$\frac{t}{q_t} = \frac{1}{k_2 q_e^2} + \frac{1}{q_e} t \quad (4)$$

$$q_t = k_d \sqrt{t} \quad (5)$$

Where q_t is the quantity of INH adsorbed during time interval t, q_e is the quantity of INH adsorbed when equilibrium is reached, k_1 is the pseudo-first-order constant, k_2 is the pseudo-second-order constant, and k_d is the adsorption-diffusion constant.

2.3. Release tests

The release of INH was assessed for three chosen clays, since they presented different pore volume resulting in different adsorption kinetics, as will be elaborated in section 3. These analyses were performed to mimic the conditions of oral drug administration. For a proper comparison, different amounts of drug containing clays were used, thus keeping the amount of INH constant. That amount was placed inside a dialysis tubing cellulose membrane that retains molecules with molecular weight up to 14,000 Da. Then, for each clay, the membrane containing the sample was immersed in a buffer solution with a pH of 7.4 to simulate the second zone of the small intestine. The release was monitored for 5 h (300 min). A sample was withdrawn after the first 10 min followed by a sample every of 30 min afterwards, making for 12 samples. After withdrawing each sample, the total volume of the solution

Table 1
Clay samples used in this work.

Analyte	CL	LP	VL	VC	VR	VVm	VVd
Name	Cloisite	Laponite	Verde Lago	Verde Claro	Verde Rosa	Verde Vermelho	Verde Verde
Type	Natural clay	Synthetic			Raw clay		
Country and/or Company	United States/BYK Additives and Instruments	United States/BYK Additives and Instruments	Argentina	Brazil	Brazil	Brazil	Brazil

was kept constant by adding the proper amount of the buffer solution.

2.4. Release data analysis

The obtained release data were fitted to two different release models: Korsmeyer-Peppas (Eq. 6) and Higuchi (Eq. 7). Where M_t is the amount of INH released after each interval (t), M_∞ is the amount of INH in the beginning of the experiment, K and n are Korsmeyer-Peppas constants, and K_h is the Higuchi constant.

$$\frac{M_t}{M_\infty} = K \bullet t^n \tag{6}$$

$$\frac{M_t}{M_\infty} = K_h \bullet t^{0.5} \tag{7}$$

To compare the release profile of the three clays, the commonly used similarity factor (f_2) was calculated (Eq. 8). This factor is proportional to the logarithmic reciprocal square root of the sum of squared differences between two distinct samples. It is widely accepted and employed for comparing dissolution profiles, aligning with FDA (Food and Drug Administration) and EMA (European Medicines Agency) guidelines (Muselík et al., 2021; Tekmen et al., 2006). Where $C1_t$ is the dissolution value of the respective first clay batch at time t, $C2_t$ is the dissolution value of the second clay batch at time t, and n is the number of sampling time points.

$$f_2 = 50 \bullet log\left\{\left[1 + \frac{1}{n}\sum_{t=1}^{n}(C1_t - C2_t)^2\right]^{-0.5} \bullet 100\right\} \tag{8}$$

As the similarity factor (f_2) is used to compare two different dissolution profiles at a time, to compare the three release profiles studied in this work, they were separated in three pairs: CL-LP, CL-VVd, and LP-VVd. In this way, it was possible to verify which clays present the most similar release profile among them. Two different release systems were considered similar when the value of the similarity factor (f_2) was in the range between 50 and 100 (Muselík et al., 2021; Tekmen et al., 2006).

2.5. Hybrid characterization

To further elucidate the influence of the clay's pore volume on controlled release, clays were characterized regarding the clay/INH interaction. TGA was used to verify the presence of INH; Fourier transformation Infrared spectroscopy (FTIR) was used to verify the interaction between the drug and the clay; and XRD was used to verify whether the drug intercalated between the clay lamellas or not.

For TGA, a Pyris Diamond TG/DTA by Perkin Elmer was used to verify the mass loss of the pristine clay and its respective hybrid. The experiments were performed under an air flow of 100 mL/min, and a temperature range of 40 to 800 °C for clays and clay/INH hybrids, and 40 to 600 °C for pure INH. The temperature was varied at a rate of 10 °C/min.

The FTIR spectra were obtained using a PerkinElmer Spectrum Two FT-IR spectrometer and the analyses were performed in the range of wavenumber of 4000 cm^{-1} to 600 cm^{-1} with 4 cm^{-1} of resolution.

XRD patterns were obtained using a Malvern Panalytical Empyrean DY-2516 X-ray diffractometer system equipped with kCu_α radiation. Scans were recorded in the range of $2\Theta = 3° - 30°$ at 1°/min.

3. Results and discussion

3.1. Clay samples characterization

The chemical composition of the six samples used in this study is listed in Table 2. Except for the two commercial samples, CL and LP, the clays contain accessory minerals, with kaolinite being the most common. The composition of LP was the most different from the others, since its structure is similar to that of the hectorite group, except that it is a synthetic clay (BYK Additives and Instruments, 2014). Different from MMT, in the hectorite group, the octahedron sheet is composed mostly of MgO instead of Al_2O_3. In part of the hectorite crystal, the MgO is replaced by Li_2O, while in MMT, Al_2O_3 is replaced by Fe_2O_3. This explains the lower concentrations of Al_2O_3 and Fe_2O_3 in LP compared to the other clays (Brigatti et al., 2006). It was noted that, in all studied clays, the presence of potentially harmful impurities, such as Mn, Ti, P, Pb, and Cd was minimal. This is important for their use in drug release systems.

In Fig. 2, the N_2 adsorption and desorption curves, shows that the studied clays manifest a type IV physisorption curve, indicating hysteresis looping. At a relative pressure (P/P_o) around 0.2, the N_2 monolayer coverage was complete and a multilayer N_2 adsorption started (Sing et al., 1985). The hysteresis looping started after (P/P_o) 0.4 indicating that, under higher relative pressure, adsorption was driven by capillary condensation. At a lower relative pressure, the hysteresis disappeared, and the adsorption occurs by Van der Waals forces (Chang et al., 2022). The morphology of clay pores was given by IUPAC classification, according to the type of hysteresis looping between the adsorption and desorption curves. It was observed that, except for LP, which exhibited H2 hysteresis type, all other clays followed a H3 type. The presence of H2 hysteresis indicated that the sample contained an abundance of ink bottle-like pores, while H3 indicated that the sample is composed of aggregates of plate-like particles, generating split shape pores (Sing et al., 1985).

According to Sing et al. (1985), the presence of macropores affects the shape of N_2 adsorption/desorption curve. If no macropores are present, the curve maintains a nearly horizontal trajectory. In contrast,

Table 2
Clay minerals, chemical composition, and pore volume of clay samples.

Analyte	CL	LP	VL	VC	VR	VVm	VVd
Clay minerals	Smectite	Smectite	Smectite, kaolinite, quartz, calcite	Smectite, quartz, albite, gibbsite	Smectite, kaolinite	Smectite, kaolinite	Smectite, kaolinite
SiO_2 (%)	59.50	58.30	61.60	56.20	55.20	56.10	56.20
Al_2O_3 (%)	21.30	0.11	19.00	19.30	24.10	21.10	21.10
Fe_2O_3 (%)	4.24	<0.10	4.61	6.03	6.41	7.94	7.94
MnO (%)	<0.10	<0.10	<0.10	<0.10	<0.10	<0.10	<0.10
MgO (%)	2.37	27.20	3.01	2.31	3.23	3.80	3.60
CaO (%)	0.47	0.14	1.31	3.49	0.19	0.23	0.21
Na_2O (%)	3.84	2.93	3.06	0.24	0.11	<0.10	<0.10
K_2O (%)	<0.10	<0.10	0.40	0.90	<0.10	<0.10	<0.10
TiO_2 (%)	0.12	<0.10	0.31	0.65	0.11	0.22	0.75
P_2O_5 (%)	<0.10	<0.10	<0.10	<0.10	<0.10	<0.10	<0.10
Ignition loss (%)	7.03	11.00	6.15	10.70	10.90	10.30	10.30
Pb (ppm)	52	1	40	54	36	33	33
Cd (ppm)	<6	<6	<6	<6	<6	<6	<6

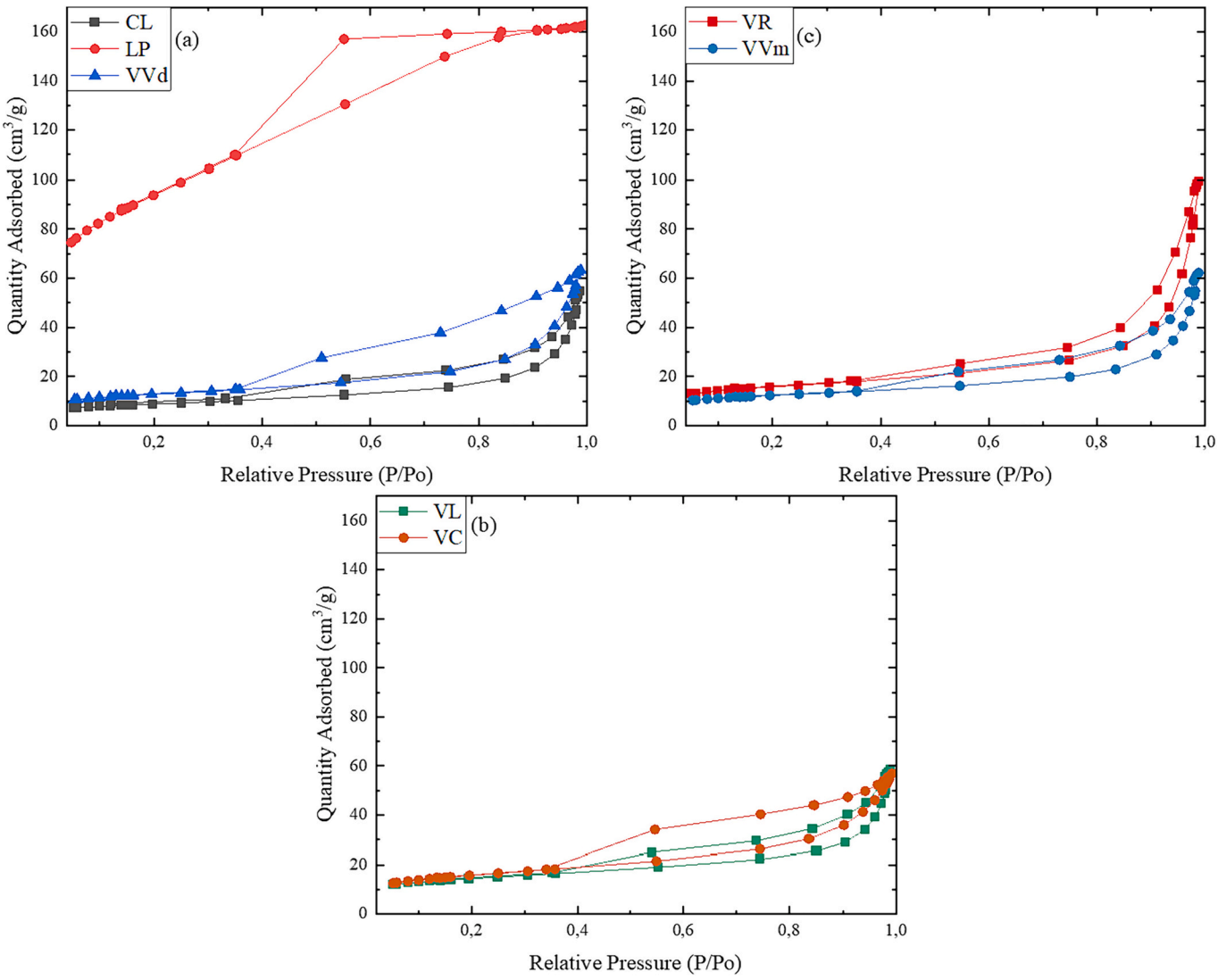

Fig. 2. N_2 adsorption/desorption curves of the seven clays used in this work.

the presence of a broad range of macropores culminates in a sharply vertical rise at a relative pressure close to 1. The curves' shape of the studied clays suggested that they are mesoporous solids. The curves' sections below P/Po 0.35 and above 0.95 suggested the presence of micropores and macropores, respectively (Shah et al., 2018).

3.2. Drug adsorption studies

Figure 3 shows that for all six clays in this study, absorption approached a plateau after three hours confirming that the choice of 24 h was more than adequate. Similar behavior was obtained by Carazo et al. (2018b), Damasceno Junior et al. (2019), and Souza et al. (2021). The three sets of experiments exhibited a low standard deviation despite the non-purified character of most clays. The absorption capacity varied from 15 mg/g (LP) to 47 mg/g (VVd) depending on the clay used.

For a wide range of adsorption efficiency, all the clays tested in this study fitted better to the pseudo-second-order model (PSO), as evidenced by R^2 values >0.930 (Table 3). Pseudo-first-order model (PFO) showed a good fit only for two clays (VVm and VVd), and adsorption-diffusion model (ADM) did not fit well in any of them (R^2 lower than 0.550 to most clays). This observation was consistent with previous studies and suggested that adsorption occurred via filling of active sites within the clays, rather than the formation of a surface layer (Souza et al., 2021).

The amount of INH that was adsorbed by clay was confirmed by TGA analysis, Fig. 4 shows the mass loss as a function of temperature for INH, pristine clay, and hybrid clay/INH. Two different typical TG curves of clay/INH samples can be seen, in this case, it shows CL (which had similar behavior to VC) and VVd (which had similar behavior to VL, VR, VVm, and LP). For all the samples, the pristine clay presented similar behavior of weight loss: the first step around 100 °C due to the surface water loss; a gradual loss followed up to 400 °C due to the loss of water of hydration and above 400 °C a sudden increase in loss occurred due to the dihydroxylation. In general, except for VC, the clays manifested just two DTG peaks related to the surface water loss and dihydroxylation process, as the sharpest events.

INH showed one-step-degradation with no residue at 600 °C, 5% of weight loss occurred around 220 °C, and the degradation was complete around 360 °C. Comparing the hybrid clay/INH and its respective pristine clay, CL and VC were the only two samples in which the pristine clay presented less surface water than its respective hybrid. Water and INH molecules were, probably, competing for being adsorbed (Giles and Smith, 1974). Therefore, the quantity of initial water molecules on the clay surface should decrease in the presence of INH. Similar results were shown in other studies (Souza et al., 2021). For CL and VC, however, it seemed that water molecules were more attracted to the clays than INH.

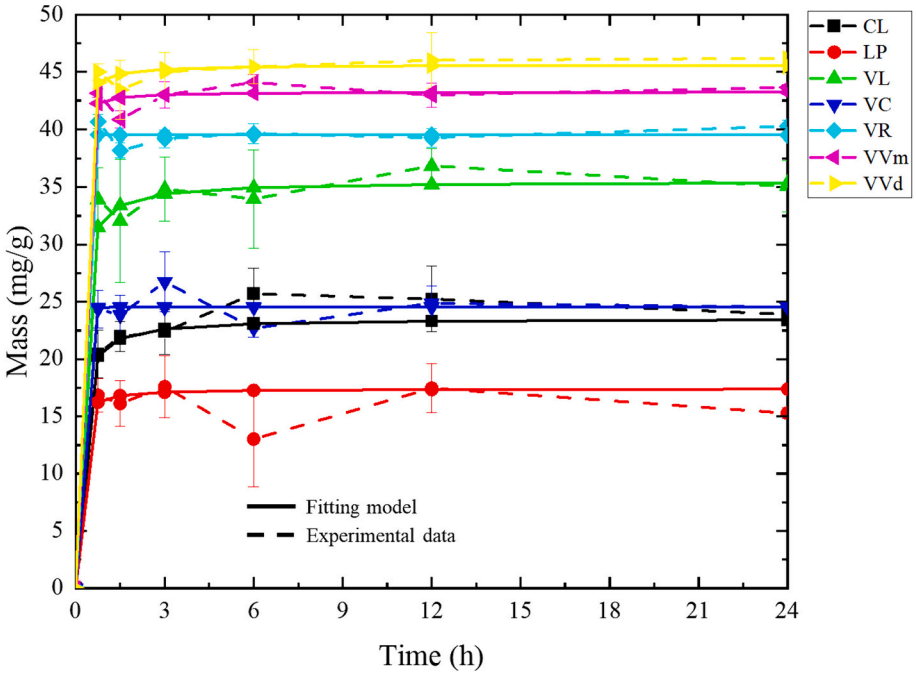

Fig. 3. PSO fitting of kinetics studies of clays.

Table 3
Parameters for PFO, PSO, and ADM fitting for each clay sample.

Samples		CL	LP	VL	VC	VR	VVm	VVd
PFO	R^2	0.869	0.088	0.225	0.001	0.059	0.995	0.994
	k_1	0.212	0.068	0.276	0.001	0.010	0.018	0.025
	q_e	25.057	17.354	44.054	24.447	39.512	43.246	45.603
PSO	R^2	0.984	0.933	0.994	0.983	0.997	0.997	0.997
	k_2	0.352	1.049	0.296	99.741	99.741	1.290	0.828
	q_e	23.549	17.429	35.528	24.538	39.521	43.275	45.639
ADM	R^2	0.445	0.104	0.531	0.002	0.059	0.220	0.550
	k_d	7.407	5.174	7.799	6.624	6.936	8.954	7.242

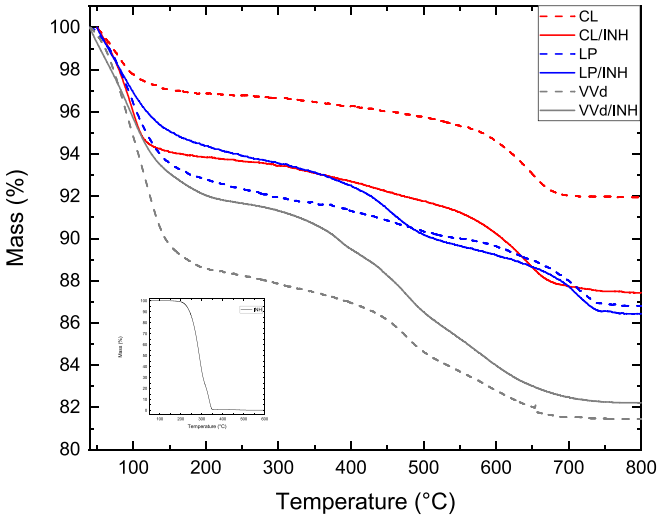

Fig. 4. TGA curves for INH, CL, CL/INH, VVd, and VVd/INH.

Table 4 presents the mass loss corresponding to different temperatures as shown by DTG peaks for each clay and its respective hybrid. Only CL and VC hybrids did not present an additional peak corresponding to INH degradation. However, their hybrid weight loss was higher than the pristine clay for temperatures above 400 °C, indicating INH degradation in this temperature range. For the other samples, the peak corresponding to INH degradation occurred at temperatures above 380 °C. The shift of the INH degradation peak indicated that the drug was protected by the clays. Similar results were shown by Carazo et al. (2018b).

The interaction between INH and clay was studied by FTIR and XRD analyses. Typical spectra of the obtained clay, clay/INH, and INH are presented in Fig. 5, which show that for pristine clays a band around 3470 cm^{-1} appeared due to the deformation of the OH group of Si-OH bonds, since they were phyllosilicates (Carazo et al., 2018b). As LP was the only sample that contains Mg^{+2} instead of Al^{+3} in its structure, it did not have the typical bands of dioctahedral smectites (3621 cm^{-1}) as it is trioctahedral type (Kiaee et al., 2022). The other bands were presented in almost all samples due to the OH and SiO vibration bands. Some interesting observations can be made, such as the fact that only CL and VC have Al^{+3} replaced by Mg^{+2} in their structure, while in VL, VR, VVm, and VVd, Al^{+3} is replaced by Fe^{+2} (Alabarse et al., 2011; Djomgoue and Njopwouo, 2013).

In the INH FTIR spectra, bands related to the hydrazine group for stretching vibrations of N—H bonds are characteristic of INH. Also, bands of C—H and C—C groups indicated the presence of the ring and the aliphatic part of this molecule (Angadi et al., 2010; Batalha et al., 2019; Carazo et al., 2018a; Carazo et al., 2018b; Damasceno Junior et al., 2019; Pandey et al., 2016).

For the hybrid spectrum, the more intense peaks were related to the

Table 4
TGA initial and final temperature and the mass loss for each stage of decomposition of clays and their respective hybrid clay/INH.

Sample	1st peak DTG		2nd peak DTG		3rd peak DTG	
	Temperature (°C)	Mass loss (%)	Temperature (°C)	Mass loss (%)	Temperature (°C)	Mass loss (%)
CL	90	3.0	637	6.5	–	–
CL/INH	103	2.3	637	10.9	–	–
VC	60	2.8	470	9.9	655	13.4
VC/INH	67	2.8	478	11.1	669	15.3
LP	94	2.7	711	12.3	–	–
LP/INH	90	2.4	452	8.7	711	12.7
VL	86	4.6	645	12.3	–	–
VL/INH	74	2.9	397	8.4	631	11.9
VR	85	4.6	475	13.9	–	–
VR/INH	70	0.8	377	8.0	481	11.5
VVm	109	6.1	484	14.0	–	–
VVm/INH	104	4.0	388	10.4	484	12.7
VVd	102	5.4	475	14.6	–	–
VVd/INH	94	4.6	384	10.1	475	12.6

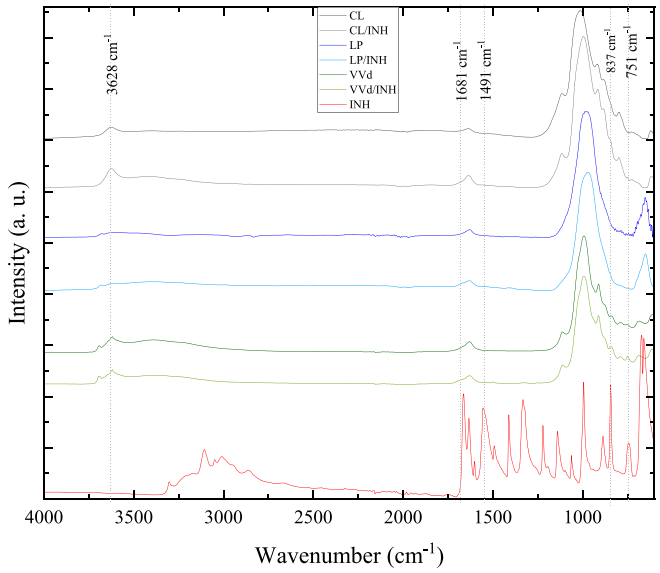

Fig. 5. FTIR spectra of INH, CL, CL/INH, LP, LP/INH, VVd, and VVd/INH.

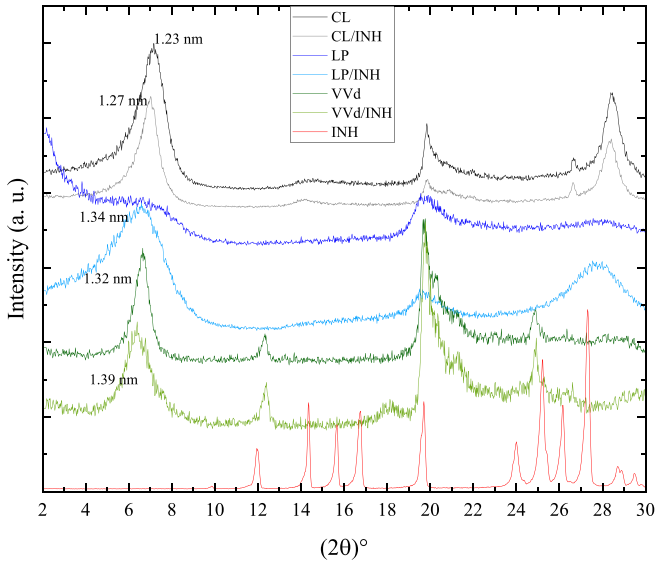

Fig. 6. XRD pattern of pristine clay, clay/INH, and INH.

clays' chemical bonds (de Almeida et al., 2019; Carazo et al., 2018b). The appearance of a deformation band around the 1660 cm^{-1} in all clays was also verified by Damasceno Junior et al. (2019), indicating the presence of INH in hybrids by the C═O folding and N—H amide group. The appearance of a band around 1431 cm^{-1} indicated ring C—C symmetric stretching of INH molecules. At the 730 cm^{-1} and 831 cm^{-1} bands, there were some differences between the pristine clay and its respective hybrid, indicating an interaction of the INH ring and clays mentioned by Damasceno Junior et al. (2019).

The XRD patterns of the original clay and the clay/INH hybrid showed no significant differences, and a typical pattern can be seen in Fig. 6. There was no increase in the basal distance after the incorporation of INH, suggesting that INH molecules did not penetrate the interlayer space. Rather, they were likely adsorbed onto the surface pores of the clay minerals. Similar behavior was observed for tetracycline by Li et al., 2010. Various studies on INH incorporation in clay minerals, however, reported increases in basal distance, indicating that each sample may behave differently, possibly depending on the adsorption parameters (pH, drug concentration, or temperature of the solution, for example (Akyuz and Akyuz, 2008; de Almeida et al., 2019)).

XRD characterization indicated that INH was not in the interlamellar space. However, FTIR results showed an interaction between the pyridine ring with silicon oxide present in the clay structure. Also, TGA results seemed to indicate that the drug was incorporated and surrounded by clay particles as suggested by Carazo et al. (2018b). Besides that, the clays with a smaller pore volume did not present a DTG peak due to the INH degradation, indicating that the INH weight loss occurred simultaneously with the dihydroxylation process.

A graph of the adsorption efficiency as a function of the pore volume, for the different clays, indicates a correlation between the pore volume of the clays and the clay's ability to adsorb INH (Fig. 7). The graph suggested that an optimal pore volume of around 0.100 cm^3/g was optimal to achieve the highest efficiency of adsorption. For clays with lower pore volumes, the adsorption was, likely, hindered by the lower rate of diffusion of the drug molecules through clay galleries, where INH solution might have difficulty penetrating them. On the other hand, for clays with higher pore volumes, the physical or chemical bonding between adsorbate and adsorbent might impede the entrapment of the drug in the pores or on the active sites.

As the pore volume seemed to be the key characteristic governing the adsorption of INH, the effect of pore volume on the release of INH was also studied. To that effect, the release of three hybrids LP/INH (pore volume of 0.250 cm^3/g), CL/INH (0.081 cm^3/g), and VVd/INH (0.097 cm^3/g) were investigated, as shown in Fig. 8. As it can be seen, the LP, which presented the highest pore volume, had the highest release rate in the first 90 min; also, it showed the highest cumulative release. On the other hand, CL and VVd presented a lower release rate during the same period, which corroborated the influence of pore volume on the

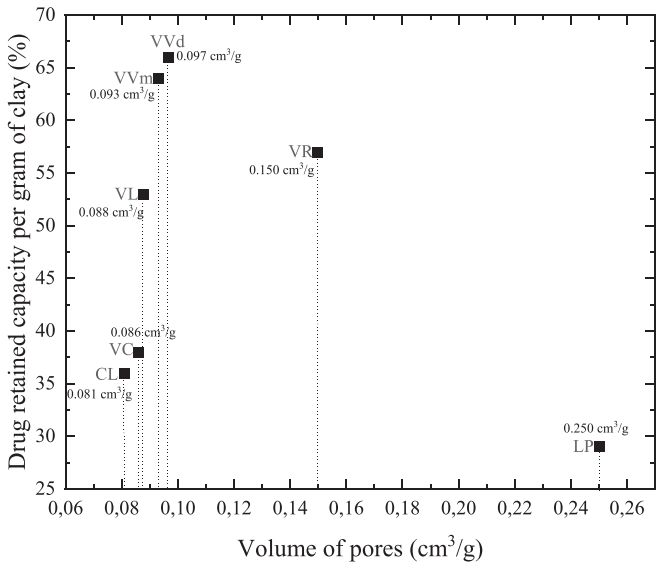

Fig. 7. Correlation between the volume of pores and efficiency of adsorption.

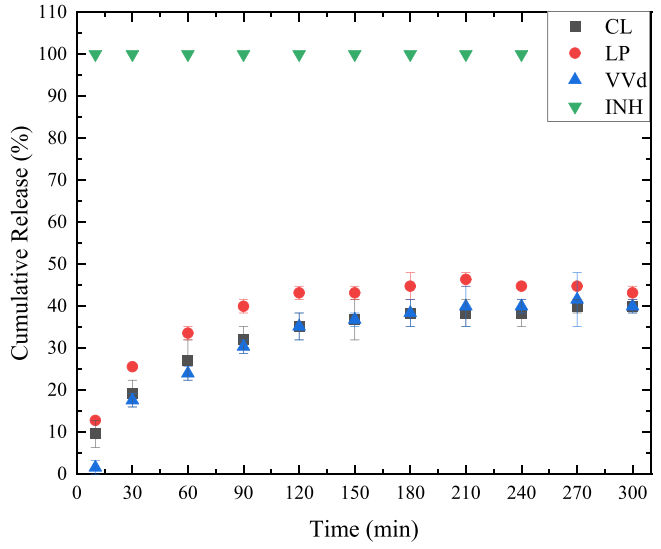

Fig. 8. Release profile of INH by pristine drug, CL, LP, and VVd at pH 7.4.

adsorption and release. After 240 min, the cumulative release into the environment for all three clays did not change, which meant that after this time, the clays were not releasing any more drugs.

The fitting parameters of the release data to two mathematical models: Korsmeyer-Peppas and Higuchi, are presented in Table 5. According to Korsmeyer-Peppas model, since n was lower than 0.5 for all clays, the release follows Fick's first law, which meant that diffusion was the driving force of this release (Korsmeyer et al., 1983).

Corroborating the release fitting results, the similarity factor (f_2), showed in Table 6, was higher than 50 for all three compared pairs. This indicated similarity of the three release profiles. The strongest similarity was observed in CL-VVd pair, the clay samples that had closer values of pore volume (0.081 and 0.097 cm^3/g, respectively) compared to the other pairs which had LP (0.250 cm^3/g). It was noteworthy that the main difference in behavior among these clays occurred at the start of the release, while past the 180-min mark, they achieved similar plateaus in their release patterns.

Table 5
Results of release fitting for CL, LP, and VVd at pH 7.4 in two different models Korsmeyer-Peppas and Higuchi.

Sample	Korsmeyer-Peppas			Higuchi	
	R^2	n	K	R^2	K_H
CL	0.975	0.238	14.533	0.947	4.269
LP	0.931	0.218	19.226	0.957	5.428
VVd	0.970	0.125	23.244	0.898	4.095

Table 6
Similarity factor (f_2) of the dissolution profile of samples.

Comparison Pair of Dissolution Profile	Similarity factor (f_2)
CL-LP	59.7
CL-VVd	76.3
LP-VVd	56.3

4. Conclusion

It was found that isoniazid can be efficiently incorporated into clay minerals to obtain a gradual drug release system. Seven smectite clays, six of which are of natural origin, and one synthetically produced, Laponite (LP), were investigated to elucidate their adsorption/retention and release behavior. Under neutral pH conditions, time dependent adsorption curves were obtained showing that three hours was enough to reach the adsorption capacity plateau, with a maximum value of 46 mg/g. Under these conditions, as evidenced by XRD, it was shown, that the drug did not penetrate the clay interlamellar space. It rather located in the pores between the tactoids of the clays. A pore volume of around 0.100 cm^3/g was found to be optimal for highest adsorption. Three clays with pores volume of 0.081, 0.097, and 0.250 cm^3/g were further investigated to determine the release mechanism, at a pH of 7.4. Since the results showed a correlation between clay's pore volume influences on clay drug adsorption capacity, it is strongly recommended for future research to include measurements of clay's pore volume.

A study of the influence of pH, temperature, and initial drug concentration on the adsorption and release process is recommended.

CRediT authorship contribution statement

Jessica de Carvalho Arjona: Writing – review & editing, Writing – original draft, Visualization, Validation, Software, Methodology, Investigation, Formal analysis, Data curation, Conceptualization. **Carina Ulsen:** Writing – review & editing, Validation, Methodology, Formal analysis. **Francisco Rolando Valenzuela-Diaz:** Writing – review & editing, Supervision, Project administration, Funding acquisition, Conceptualization. **Nicole Raymonde Demarquette:** Writing – review & editing, Writing – original draft, Validation, Supervision, Resources, Project administration, Methodology, Funding acquisition, Conceptualization.

Declaration of competing interest

The authors declare that they have no known competing financial interests or personal relationships that could have appeared to influence the work reported in this paper.

Data availability

Data will be made available on request.

Acknowledgements

This work was supported by the CNPq (Conselho Nacional de

Desenvolvimento Científico e Tecnológico), grant number 141859/2020-2; CAPES (Coordenação de Aperfeiçoamento de Pessoal de Nível Superior), grant number 88887.694663/2022-00; FAPESP (Fundação de Amparo à Pesquisa do Estado de São Paulo), grant number 2019/01231-2; and NSERC (Natural Sciences and Engineering Research Council of Canada), grant number ALLRP 573019-22.

The authors also would like to acknowledge and express gratitude for the financial and infra structural assistance provided by PMT (Department of Metallurgical and Materials Engineering at USP), LCT (*Laboratório de Caracterização Tecnológica* at USP), LIPEC-PolymerETS (*Laboratoire d'ingénierie des polymères et composites* at ÉTS), and STEPPE (*Station Expérimentale des Procédés Pilotes en Environnement* at ÉTS). As well to the research associate Dr. Mazen Samara for the writing assistance and Dr. Maria das Graças Silva-*V*alenzuela for her expertise and assistance throughout this study.

Appendix A. Supplementary data

Supplementary data to this article can be found online at https://doi.org/10.1016/j.clay.2024.107341.

References

Akyuz, S., Akyuz, T., 2008. FT-IR and FT-Raman spectroscopic studies of adsorption of isoniazid by montmorillonite and saponite. Vib. Spectrosc. 48 (2), 229–232. https://doi.org/10.1016/j.vibspec.2008.02.019.

Alabarse, F.G., Conceição, R.V., Balzaretti, N.M., Schenato, F., Xavier, A.M., 2011. In-situ FTIR analyses of bentonite under high-pressure. Appl. Clay Sci. 51 (1–2), 202–208. https://doi.org/10.1016/j.clay.2010.11.017.

de Almeida, J.M.F., Damasceno Júnior, E., Verrísimo, L.M., Fernandes, N.S., 2019. pH-dependent release system of isoniazid carried on nanoparticles of silica obtained from expanded perlite. Appl. Surf. Sci. 489, 297–312. https://doi.org/10.1016/j.apsusc.2019.05.317.

Angadi, S.C., Manjeshwar, L.S., Aminabhavi, T.M., 2010. Interpenetrating polymer network blend microspheres of chitosan and hydroxyethyl cellulose for controlled release of isoniazid. Int. J. Biol. Macromol. 47 (2), 171–179. https://doi.org/10.1016/j.ijbiomac.2010.05.003.

Avnir, David, Jaroniec, Mieczyslaw, 1989. An isotherm equation for adsorption on fractal surfaces of heterogeneous porous materials. Langmuir 5, 1431–1433. https://pubs.acs.org/sharingguidelines.

Batalha, I.L., Bernut, A., Schiebler, M., Ouberai, M.M., Passemar, C., Klapholz, C., Kinna, S., Michel, S., Sader, K., Castro-hartmann, P., Renshaw, S.A., Welland, M.E., Floto, R.A., 2019. Polymeric nanobiotics as a novel treatment for mycobacterial infections. J. Control. Release 314 (October), 116–124. https://doi.org/10.1016/j.jconrel.2019.10.009.

Bhat, A.H., Rangreez, T.A., Inamuddin, Chisti, H.-T.-N., 2020. Wastewater treatment and biomedical applications of montmorillonite based nanocomposites: a review. Curr. Anal. Chem. 18 (3), 269–287. https://doi.org/10.2174/1573411016999200729123309.

Borrego-Sánchez, A., Sainz-Díaz, C.I., Perioli, L., Viseras, C., 2021. Theoretical study of retinol, niacinamide and glycolic acid with halloysite clay mineral as active ingredients for topical skin care formulations. Molecules 26 (15). https://doi.org/10.3390/molecules26154392.

Brigatti, M.F., Galan, E., Theng, B.K.G., 2006. Chapter 2 structures and mineralogy of clay minerals. In: Bergaya, F., Theng, B.K.G., Lagaly, G. (Eds.), Handbook of Clay Science, vol. 1. Elsevier, pp. 19–86. https://doi.org/10.1016/S1572-4352(05)01002-0.

BYK Additives & Instruments, 2014. Laponite: performance additives. In: Technical information B-RI 21.

Carazo, E., Borrego-Sánchez, A., García-Villén, F., Sánchez-Espejo, R., Aguzzi, C., Viseras, C., Sainz-Díaz, C.I., Cerezo, P., 2017. Assessment of halloysite nanotubes as vehicles of isoniazid. Colloids Surf. B: Biointerfaces 160, 337–344. https://doi.org/10.1016/j.colsurfb.2017.09.036.

Carazo, E., Borrego-Sánchez, A., García-Villén, F., Sánchez-Espejo, R., Viseras, C., Cerezo, P., Aguzzi, C., 2018a. Adsorption and characterization of palygorskite-isoniazid nanohybrids. Appl. Clay Sci. 160, 180–185. https://doi.org/10.1016/j.clay.2017.12.027.

Carazo, E., Borrego-Sánchez, A., Sánchez-Espejo, R., García-Villén, F., Cerezo, P., Aguzzi, C., Viseras, C., 2018b. Kinetic and thermodynamic assessment on isoniazid/montmorillonite adsorption. Appl. Clay Sci. 165, 82–90. https://doi.org/10.1016/j.clay.2018.08.009.

Carazo, E., Sandri, G., Cerezo, P., Lanni, C., Ferrari, F., Bonferoni, C., Viseras, C., Aguzzi, C., 2019. Halloysite nanotubes as tools to improve the actual challenge of fixed doses combinations in tuberculosis treatment. J. Biomed. Mater. Res. - Part A 107 (7), 1513–1521. https://doi.org/10.1002/jbm.a.36664.

Chang, J., Fan, X., Jiang, Z., Wang, X., Chen, L., Li, J., Zhu, L., Wan, C., Chen, Z., 2022. Differential impact of clay minerals and organic matter on pore structure and its fractal characteristics of marine and continental shales in China. Appl. Clay Sci. 216 https://doi.org/10.1016/j.clay.2021.106334.

Damasceno Junior, E., de Almeida, J.M.F., Silva, I. do N., Moreira de Assis, M.L., dos Santos, L.M., Dias, E.F., Bezerra Aragão, V.E., Veríssimo, L.M., Fernandes, N.S., da Silva, D.R., Junior, E.D., Mayara, J., De Almeida, F., Silva, N., Lizandra, M., De Assis, M., Maciel, L., Dias, E.F., Eduardo, V., Ribeiro, D., 2019. pH-responsive release system of isoniazid using palygorskite as a nanocarrier. J. Drug Deliv. Sci. Technol. 55 (October 2019), 101399 https://doi.org/10.1016/j.jddst.2019.101399.

Djomgoue, P., Njopwouo, D., 2013. FT-IR spectroscopy applied for surface clays characterization. J. Surf. Eng. Mater. Adv. Technol. 03 (04), 275–282. https://doi.org/10.4236/jsemat.2013.34037.

Feng, D., Li, X., Wang, X., Li, J., Sun, F., Sun, Z., Zhang, T., Li, P., Chen, Y., Zhang, X., 2018. Water adsorption and its impact on the pore structure characteristics of shale clay. Appl. Clay Sci. 155 (February), 126–138. https://doi.org/10.1016/j.clay.2018.01.017.

Giles, C.H., Smith, D., 1974. A general treatment and classification of the solute adsorption isotherm. J. Co 47 (3), 755–765. https://doi.org/10.1007/s41193-016-0111-5.

Kiaee, G., Dimitrakakis, N., Sharifzadeh, S., Kim, H.J., Avery, R.K., Moghaddam, K.M., Haghniaz, R., Yalcintas, E.P., de Barros, N.R., Karamikamkar, S., Libanori, A., Khademhosseini, A., Khoshakhlagh, P., 2022. Laponite-based nanomaterials for drug delivery. In: Advanced Healthcare Materials, vol. 11, Issue 7. John Wiley and Sons Inc., pp. 1–21. https://doi.org/10.1002/adhm.202102054

Korsmeyer, R.W., Gurny, R., Doelker, E., Buri, P., Peppas, N.A., 1983. Mechanisms of solute release from porous hydrophilic polymers. Int. J. Pharm. 15 (1), 25–35. https://doi.org/10.1016/0378-5173(83)90064-9.

Li, Z., Chang, P.H., Jean, J.S., Jiang, W.T., Wang, C.J., 2010. Interaction between tetracycline and smectite in aqueous solution. J. Colloid Interface Sci. 341 (2), 311–319. https://doi.org/10.1016/j.jcis.2009.09.054.

Muselík, J., Komersová, A., Kubová, K., Matzick, K., Skalická, B., 2021. A critical overview of FDA and EMA statistical methods to compare in vitro drug dissolution profiles of pharmaceutical products. Pharmaceutics 13 (10). https://doi.org/10.3390/pharmaceutics13101703.

Nicola, B.P., Bernardo-Gusmão, K., Schwanke, A.J., 2021. Smectite Clay Nanoarchitectures: Rational Design and applications. In: L. M, Vasilievna, K.B.I. Kharissova Oxana, Torres-Martínez (Eds.), Handbook of Nanomaterials and Nanocomposites for Energy and Environmental Applications. Springer International Publishing, pp. 275–305. https://doi.org/10.1007/978-3-030-36268-3_60.

Pandey, G., Yadav, S.K., Mishra, B., 2016. Preparation and characterization of isoniazid and lamivudine co-loaded polymeric microspheres, 44 (8), 1867–1877.

Peng, Q., Xu, P., Xiao, S., 2018. Porous Laponite/Poly(L-lactic acid) membrane with controlled release of TCH and efficient antibacterial performance. Fibers Polymers 19 (3), 477–488. https://doi.org/10.1007/s12221-018-7925-5.

Perrie, Y., Rades, T., Graeser, K., 2019. Principles of controlled release. In: Hillery, A.M., Park, K. (Eds.), Drug Delivery: Fundamentals & Applications, 2nd ed. Taylor & Francis, pp. 25–46. https://doi.org/10.1201/9781315382579.

Reinholdt, M.X., Hubert, F., Faurel, M., Tertre, E., Razafitianamaharavo, A., Francius, G., Prêt, D., Petit, S., Béré, E., Pelletier, M., Ferrage, E., 2013. Morphological properties of vermiculite particles in size-selected fractions obtained by sonication. Appl. Clay Sci. 77–78, 18–32. https://doi.org/10.1016/j.clay.2013.03.013.

Sciascia, L., Calabrese, I., Cavallaro, G., Merli, M., Scialabba, C., Liveri, M.L.T., 2021. Modified montmorillonite as drug delivery agent for enhancing antibiotic therapy. Minerals 11 (12). https://doi.org/10.3390/min11121315.

Shah, L.A., da Silva Valenzuela, M. das G., Ehsan, A.M., Valenzuela Díaz, F.R., Khattak, N.S., 2013. Characterization of Pakistani purified bentonite suitable for possible pharmaceutical application. Appl. Clay Sci. 83–84, 50–55. https://doi.org/10.1016/j.clay.2013.08.007.

Shah, L.A., Silva Valenzuela, M. das G. da, Farooq, M., Khattak, S.A., Valenzuela Díaz, F. R., 2018. Influence of preparation methods on textural properties of purified bentonite. Appl. Clay Sci. 162, 155–164. https://doi.org/10.1016/j.clay.2018.06.001.

Sing, K.S.W., Everett, D.H., Haul, R.A.W., Moscou, L., Pierotti, R.A., Rouquérol, J., Siemieniewska, T., 1985. reporting physisorption data for gas/solid systems. Pure Appl. Chem. 57 (4), 603–619.

Souza, I.M.S., Sainz-Díaz, C.I., Viseras, C., Pergher, S.B.C., 2020. Adsorption capacity evaluation of zeolites as carrier of isoniazid. Microporous Mesoporous Mater. 292 https://doi.org/10.1016/j.micromeso.2019.109733.

Souza, I.M.S., Borrego-Sánchez, A., Sainz-Díaz, C.I., Viseras, C., Pergher, S.B.C., 2021. Study of Faujasite zeolite as a modified delivery carrier for isoniazid. Mater. Sci. Eng. C 118, 12. https://doi.org/10.1016/j.msec.2020.111365.

Tan, K.L., Hameed, B.H., 2017. Insight into the adsorption kinetics models for the removal of contaminants from aqueous solutions. J. Taiwan Inst. Chem. Eng. 74, 25–48. https://doi.org/10.1016/j.jtice.2017.01.024.

Tekmen, I., Sönmez, Ü., Kırılmaz, L., Güneri, T., 2006. Evaluation of in vitro release and skin irritation of benzoyl peroxide-containing products, 16 (6).

Tiwari, G., Tiwari, R., Bannerjee, S., Bhati, L., Pandey, S., Pandey, P., Sriwastawa, B., 2012. Drug delivery systems: an updated review. Intern. J. Pharmac. Investig. 2 (1), 2–11. https://doi.org/10.4103/2230-973X.96920.

Ulsen, C., Tseng, E., Angulo, S.C., Landmann, M., Contessotto, R., Balbo, J.T., Kahn, H., 2019. Concrete aggregates properties crushed by jaw and impact secondary crushing. J. Mater. Res. Technol. 8 (1), 494–502. https://doi.org/10.1016/j.jmrt.2018.04.008.

Wang, S., Zheng, F., Huang, Y., Fang, Y., Shen, M., Zhu, M., Shi, X., 2012. Encapsulation of amoxicillin within laponite-doped poly(lactic-co-glycolic acid) nanofibers: preparation, characterization, and antibacterial activity. ACS Appl. Mater. Interfaces 4 (11), 6393–6401. https://doi.org/10.1021/am302130b.

Wang, X., Cheng, H., Chai, P., Bian, J., Wang, X., Liu, Y., Yin, X., Pan, S., Pan, Z., 2020. Pore characterization of different clay minerals and its impact on methane

adsorption capacity. Energy Fuel 34 (10), 12204–12214. https://doi.org/10.1021/acs.energyfuels.0c01922.

Zheng, L., Zhou, B., Qiu, X., Xu, X., Li, G., Lee, W.Y.W., Jiang, J., Li, Y., 2019. Direct assembly of anticancer drugs to form Laponite-based nanocomplexes for therapeutic co-delivery. Mater. Sci. Eng. C 99, 1407–1414. https://doi.org/10.1016/j.msec.2019.02.083.

Zhu, R., Chen, Q., Zhou, Q., Xi, Y., Zhu, J., He, H., 2016. Adsorbents based on montmorillonite for contaminant removal from water: A review. In: Applied Clay Science, vol. 123. Elsevier Ltd., pp. 239–258. https://doi.org/10.1016/j.clay.2015.12.024